Article

Thin-Film Composite Polyamide Membranes Decorated with Photoactive Carbon Dots for Antimicrobial Applications

Liu Yang, Jennifer C. Jackson, Camilla H. M. Camargos, Marcella Torres Maia, Diego Stéfani Teodoro Martinez, Amauri Jardim de Paula, Camila A. Rezende, and Andreia F. Faria*

Cite This: *ACS Appl. Nano Mater.* 2024, 7, 1477−1490

Read Online

ACCESS | Metrics & More | Article Recommendations | Supporting Information

ABSTRACT: In this study, we modified thin-film composite (TFC) membranes by coating them with antimicrobial and photoactive lignin-derived carbon dots (CD) using polydopamine (PDA) chemistry. The CD solution was applied to the membrane surface at different concentrations (100, 300, 500, and 1000 μg/mL) to create CD-100, CD-300, CD-500, and CD-1000 membranes. The CD-modified membranes were tested against *Escherichia coli* and *Bacillus subtilis* cells under three light conditions: darkness, simulated sunlight, and 365 nm ultraviolet (UV). The CD-500 and CD-1000 membranes showed the highest toxicity against *E. coli* and *B. subtilis* cells under UV photoactivation. However, the exceptional antibacterial properties of the CD-1000 membrane were accompanied by significant losses in the water permeability (parameter *A*) and water flux. The CD-500 membrane, on the other hand, demonstrated slightly lower toxicity than CD-1000 while maintaining the transport properties of the membrane compared to the pristine TFC. Under darkness, simulated sunlight, and UV light, the CD-500 inactivated 69.9 ± 1.7, 76.4 ± 1.8, and 99.92 ± 0.03% of attached *E. coli* cells, respectively, compared with the pristine TFC control in darkness. Prolonged pre-exposure treatments to UV light showed that the CD-500 membrane loses its antibacterial activity significantly after 9, 15, and 24 h of continuous contact with UV radiation. The CD-500 also reduces its toxicity to *E. coli* cells from 99.92 ± 0.03 to 71.4 ± 0.6% when tested in the presence of simulated wastewater compared to the results collected in saline solution under UV light. Our findings demonstrate the potential of CD for controlling bacterial attachment in TFC membranes while highlighting the need to optimize the coating design to maximize stability under UV exposure and toxicity under real-life conditions.

KEYWORDS: antimicrobial, nanomaterials, thin-film composite membranes, reverse osmosis, carbon dots, lignin
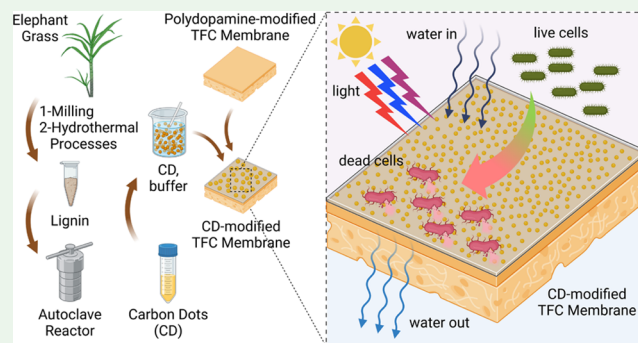
INTRODUCTION

Thin-film composite (TFC) membranes are considered the gold standard for desalination[1,2] and dominate reverse osmosis (RO) water treatment applications. RO membrane filtration has the potential to address ongoing and developing issues surrounding water scarcity[3,4] due to its excellent separation performance.[5,6] However, there are still drawbacks associated with the application of TFC membranes and RO filtration, including capital costs, energy costs, and membrane fouling. During operation, TFC membranes can become fouled in several ways due to components of the feedwater: (1) particulate fouling caused by a buildup of larger particulates and colloids on the membrane surface,[7] (2) scaling due to inorganic salt precipitation,[8] (3) organic fouling resulting from adsorption of natural organic compounds,[9] and (4) biofouling arising from the proliferation of biological species on the membrane surface.[10−12] Of these, biofouling poses the greatest concern as it cannot be controlled as readily as the other types of fouling.[13,14] The thin polyamide selective layer of the TFC

membrane provides a favorable environment for the adhesion of bacteria, proteins, and organic matter due to the roughness, hydrophobicity, and negative charge of the membrane surface. As a result, TFC membranes are highly prone to biofouling,[15−17] which causes a significant decline in water flux and an overall decrease in membrane performance.[15,18] Once membranes become heavily fouled, they must be replaced, which drives up the costs associated with RO membrane filtration.[19]
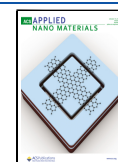
Using traditional methods of disinfection, such as chlorination, to prevent biofilm formation is not practical as the polyamide selective layer is susceptible to oxidation by
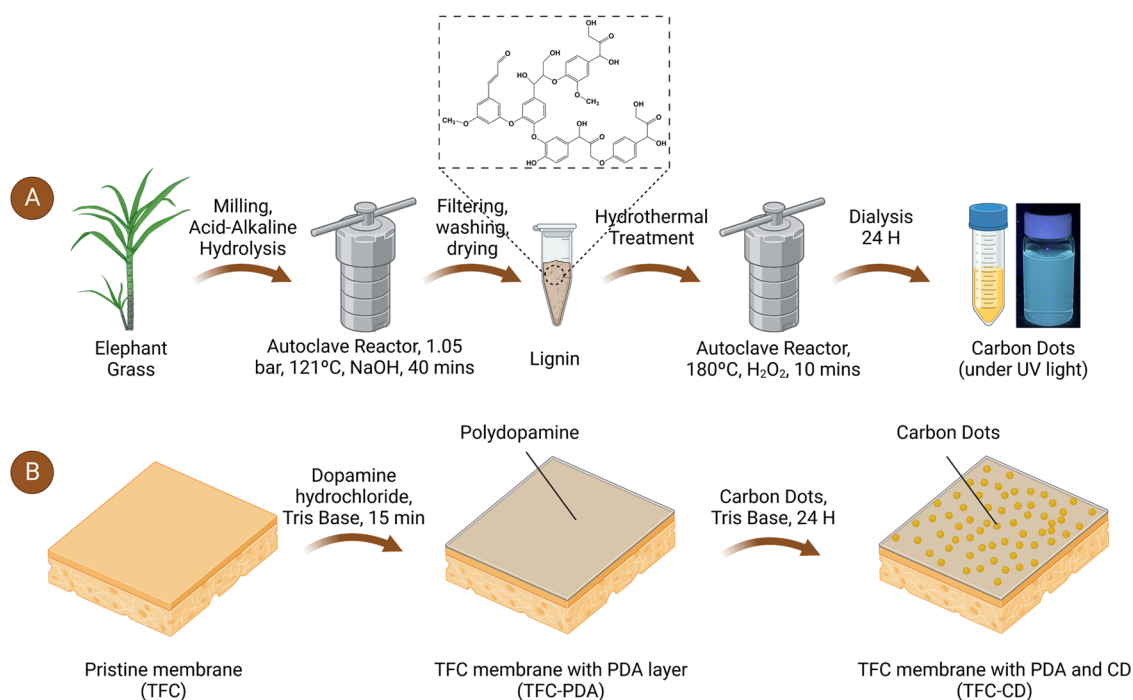
Figure 1. (A) Extraction of lignin from elephant grass (*P. purpureum*) and conversion of lignin to CD (fluorescent under UV light). (B) The membrane modification process uses the biomimetic self-polymerization reaction of dopamine to form a layer of polydopamine and subsequent attachment of CD (created with BioRender.com).

chlorine.[2,20] Disinfection with ultraviolet (UV) light alone is a potential technology for preventing biofilm formation on TFC membranes, but it is energy-demanding, and its effectiveness depends on the type of microorganism.[21−24] This highlights the need for novel approaches that address biofouling while utilizing sustainable materials.[10−12] Alternative methods, such as surface modification with bactericides, have been gaining attention to reduce the impacts of biofilms in filtration membranes.[10−12,25,26]

Carbon-based nanomaterials with unique properties have aroused growing interest as antimicrobial coatings, as they demonstrate various antibacterial effects and are less prone to induce bacterial resistance compared to traditional antibiotics.[27,28] Although representative materials such as graphene and carbon nanotubes can effectively endow TFC membranes with resistance to biofouling,[29−32] their toxicity to bacteria is limited as it requires contact[33] and their cost hinders their widespread application as antimicrobial agents.[34,35] Carbon dots (CD) are a new class of fluorescent and light-sensitive carbon nanomaterials which have been used as antimicrobials due to their highly oxidative properties.[36−38] Notably, in addition to their fluorescence emission, CD have demonstrated good optical stability[39] and exhibit antibacterial properties under photoexcitation.[40−43] Synthetic routes for CD production are also generally simple, inexpensive, and environmentally friendly.

A suitable precursor to CD is lignin, which is a renewable resource with a high carbon content. Lignin is the second-most abundant biopolymer after cellulose, and it is also a major component of plant materials (typically 15−40% dry weight in vascular plants).[44] The physicochemical properties of CD are influenced by the precursor material used for their synthesis,[45] and lignin itself possesses a myriad of beneficial physicochemical properties that may have a positive impact on the properties of the synthesized CD. For example, lignin demonstrates excellent chemical stability, thermal stability, antioxidant properties, adhesive properties, and antimicrobial behavior.[46] Furthermore, lignin poses an environmental concern due to its prevalence in waste streams[47] and recalcitrant nature.[46] Billion tons of dry lignocellulosic waste are produced globally each year,[48] which could provide a cheap and readily available feedstock. Lignin can be facilely converted into CD using a single, simple hydrothermal treatment to achieve waste utilization.[49−51]

In the present study, we demonstrate a simple and environmentally friendly route to synthesize fluorescent CD by the hydrothermal treatment of lignin with the assistance of H_2O_2. CD were thoroughly characterized, and polydopamine (PDA) chemistry was used to attach them to the TFC membrane surface. The functionalized membranes were thoroughly characterized morphologically using microscopy and spectrometry techniques, and the membrane's intrinsic transport properties were evaluated in a bench-scale RO filtration system. Membrane antimicrobial activity was tested using plate counting methods with *Escherichia coli* (Gram-negative) and *Bacillus subtilis* (Gram-positive) as model bacteria. CD imparted strong antibacterial activity to TFC membranes under solar and UV light exposure. Finally, our results highlight the potential use of CD to increase biofouling resistance in TFC membranes without detracting from membrane performance.

■ MATERIALS AND METHODS

Materials and Chemicals. Hydrogen peroxide (30%, Certified ACS), sodium chloride (Crystalline/Certified ACS), lysogeny broth (LB), agar (Powder/Flakes), sodium phosphate dibasic (anhydrous, certified ACS), sodium phosphate monobasic (anhydrous, 99%), ethanol (absolute, 200 proof, Molecular Biology grade), 3-hydroxytyramine hydrochloride (99%), and tris(hydroxymethyl) aminomethane (Tris Base, ≥99.8%) were obtained from Fisher Scientific (Atlanta,

GA). A LIVE/DEAD BacLightTM Bacterial Viability Kit was obtained from Thermo Fisher Scientific (Carlsbad, CA). Glutaraldehyde (50% aqueous solution, electron microscopy grade), paraformaldehyde (16% aqueous solution, Electron Microscopy grade), and hexamethyldisilazane (97.0%) were obtained from Electron Microscopy Sciences (Hatfield, PA). Sulfuric acid (H$_2$SO$_4$, 98%) and sodium hydroxide (NaOH, certified ACS) were obtained from Synth (Diadema, São Paulo, Brazil). Elephant grass (*Pennisetum purpureum*) was kindly supplied by the Institute of Animal Science (Instituto de Zootecnia, Nova Odessa, São Paulo, Brazil). Plants were harvested 12 months after planting. Leaves were separated, dried in a convection oven (Tecnal TE-394/3, Piracicaba, Brazil) at 60 °C for 24 h, and knife milled through a 10-mesh sieve (grinder SOLAB SL 31, Piracicaba, Brazil). Then, the milled biomass was stored in plastic bags. Thin-film composite membranes (FilmTec Flat Sheet SW30XLE membrane) were obtained from OctoChem (Vandalia, IL). Deionized (DI) water with a resistance of 18.2 MΩ·cm was obtained from a Milli-Q Direct Water Purification System (EMD Millipore, Burlington, MA). All of the solutions described were prepared using deionized water.

Preparation of Carbon Dots. CD were synthesized from the lignin of elephant grass (*P. purpureum*) leaves (Figure 1A). To obtain the lignin,[49−51] milled elephant grass leaves were treated with sequential acid-alkaline dilute hydrolysis in an autoclave (Phoenix AV-75, Araraquara, Brazil) according to previously reported methods.[52] In the first treatment, milled leaves and stems were hydrolyzed with 1% (v/v) H$_2$SO$_4$ at 121 °C and 1.05 bar for 40 min at a 1:10 solid-to-liquid ratio. Then, the biomass was washed with tap water, and solids were recovered. This acid pretreatment removes extractives and most of the hemicellulose contained in the plant biomass. Following the acid step, the recovered biomass underwent an alkali hydrothermal treatment with 2% (w/v) NaOH at the same conditions applied in the acid step (121 °C, 1.05 bar for 40 min) at a 1:20 solid-to-liquid ratio. The alkaline step extracts most of the lignin from the substrate. The lignin-rich alkaline liquors were then acidified by the dropwise addition of concentrated H$_2$SO$_4$ under constant stirring to precipitate the lignin. The isolated lignin was collected by vacuum filtration and rinsed until the rinsing water reached a pH of 6−7. The solid lignin was then oven-dried at 40 °C for 12 h and stored until use.

To prepare the carbon dot (CD) suspension, a hydrothermal process in the presence of hydrogen peroxide was performed.[51] 100 mg of dried lignin was added to 30 mL of DI water. The lignin dispersion was bath-sonicated for 45 min to disperse the lignin in the suspension better. A volume of 2 mL of 30% hydrogen peroxide was added to the dispersion, which was vortexed to mix and then transferred to a poly(tetrafluoroethylene) (PTFE) liner inside a stainless-steel autoclave. The hydrothermal treatment was carried out at 180 °C for 10 min. After the hydrothermal autoclave had cooled and depressurized, the CD suspension was vacuum-filtered through a 0.22 μm poly(vinylidene fluoride) (PVDF) filter to remove unreacted lignin. The filtrate was then dialyzed against deionized water in a dialysis membrane with a 3500 Da molecular-weight cutoff (MWCO) for 24 h to remove impurities. The purified CD suspension was stored at 4 °C until use. These processes are depicted in Figure 1A.

Characterization of Carbon Dots. The presence of CD in the suspension was initially confirmed qualitatively by focusing ultraviolet (UV) light on the solution to check for observable fluorescence. Fluorescence was confirmed quantitatively by measuring the fluorescence intensity of the CD suspension and a suspension of lignin dispersed in deionized water at an excitation wavelength of 360 nm and an emission wavelength of 450 nm. The UV−visible light absorbance profile of the CD solution was also measured. The excitation wavelength-dependent fluorescence emission spectra of the CD solution were collected at emission wavelengths of 340, 360, 365, 380, 400, 420, and 440 nm. The quantum yield of the CD was determined by using the equation given below with quinine sulfate dissolved in 0.050 M H$_2$SO$_4$ as a reference solution.

$$\Phi_{CD} = \Phi_S \times \frac{F_{CD}}{F_S} \times \frac{OD_S}{OD_{CD}} \times \frac{(\eta_{CD})^2}{(\eta_S)^2}$$

where Φ is the quantum yield, F represents the integrated fluorescence intensity, OD is the optical density (absorbance) at a specific wavelength, and η is the refractive index of the solution. The subscript CD refers to the carbon dots suspension and S refers to the standard (quinine sulfate). All fluorescence and absorbance measurements for the CD solution were taken in a CLARIOstar Plus microplate reader (BMG LABTECH, Inc., Cary, NC).

The morphological characteristics of the CD were assessed by transmission electron microscopy (TEM). A 400-mesh carbon-coated Formvar nickel grid was glow discharged using the PELCO easiGlow (Ted Pella, Redding, CA), followed by floating onto a 10 μL droplet of the provided sample for 5 min, and excess solution was drawn off with filter paper. The sample grid was then floated on a 10 μL droplet of 0.5% aqueous uranyl acetate for 30 s, and after removing the excess stain with filter paper, the sample was air-dried and examined with an FEI Tecnai G2 Spirit Twin TEM (FEI Corp., Hillsboro, OR). Digital images were acquired with a Gatan UltraScan 2k × 2k camera and Digital Micrograph software (Gatan, Inc., Pleasanton, CA). CD particle size was measured using TEM images analyzed with the ImageJ software. The size distribution is based on measurements for 62 particles.

The chemical properties of the carbon dots were evaluated by using X-ray photoelectron spectroscopy (XPS). For such, the CD suspension was lyophilized to yield a powder, and the analysis was conducted with a PHI VersaProbe III Scanning XPS Microprobe (Physical Electronics, Chanhassen, MN) using a monochromatic Al-Kα X-ray source (*hν* = 1486.7 eV). The photoelectron escape depth was less than 10 nm, and the takeoff angle for the photoelectrons was set to 45°. XPS analysis was conducted over an area of 100 μm^2 and the spectra were averaged over 5 scans.

Membrane Functionalization with CD Using PDA. Commercial TFC membranes (FilmTec Flat Sheet SW30XLE) were functionalized with CD using a well-established PDA chemistry,[53,54] as depicted in Figure 1B. The coating resulting from the deposition of PDA mimics the protein structures that mussels use to attach themselves to various surfaces.[53] By utilization of this chemistry, a layer of CD can be applied to the TFC membrane surface similarly. Membranes were laid on a glass sheet and covered with a frame made of rubber and high-density polyethylene, leaving only the active layer exposed. During functionalization, the frames were clamped to prevent leakage and placed onto an orbital shaker set to 30 rpm at room temperature. 50 mg of 3-hydroxytyramine hydrochloride was then dissolved in 25 mL of 10 mM tris(hydroxymethyl) aminomethane (Tris Base) solution at pH 8.5. This solution was left in contact with the thin-film composite membranes for 15 min to allow a thin layer of PDA to develop on the membrane surface. The solution turned brown during this process, indicating that the dopamine self-polymerization reaction was occurring and the membrane was briefly rinsed. Following this, the membrane surface was contacted with suspensions of 100, 300, 500, and 1000 μg/mL CD in 10 mM tris base at pH 8.5 for 24 h to attach different concentrations of CD to the PDA coating on the membrane surface. The CD suspension turned brown after the 24 h contact time, and the solution was discarded. The membrane was then rinsed well and stored in deionized water at 4 °C. In this study, pristine membranes (TFC) were compared to membranes modified with only a thin layer of PDA (TFC-PDA) and membranes modified with both a thin layer of PDA and subsequent CD attachment (CD-100, CD-300, CD-500, and CD-1000 membranes).

Characterization of Modified Membranes. The morphology of pristine and modified TFC membranes (CD-100, CD-300, CD-500, and CD-1000) was observed by scanning electron microscopy (SEM). Membrane coupons 1 cm^2 in size were dried overnight in a desiccator at room temperature and then attached to aluminum SEM stubs by using conductive carbon tape. The samples prepared on stubs were dried overnight in a vacuum desiccator at room temperature before
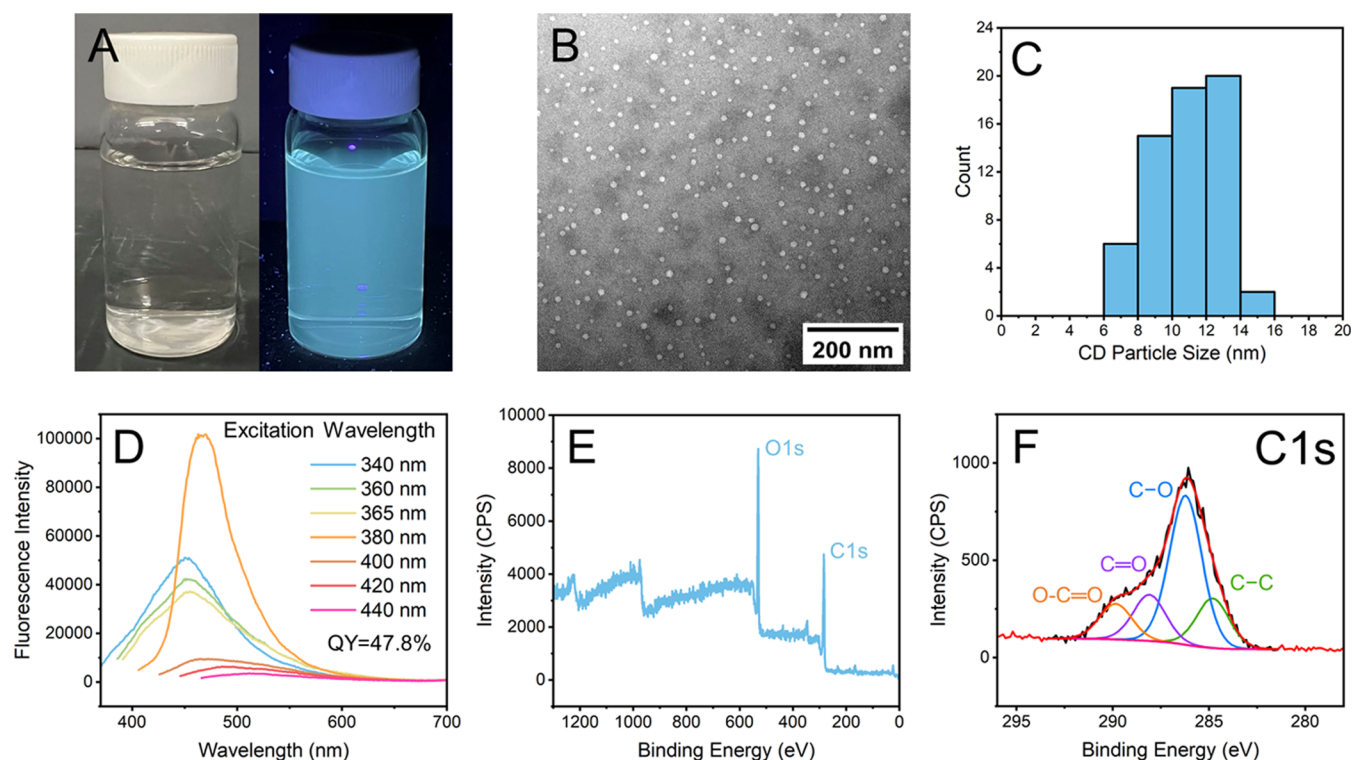
Figure 2. (A) Photograph of CD suspensions under exposure to daylight and UV light at 365 nm. (B) TEM micrograph of the dried CD suspension. (C) Size distribution of CD particles obtained from TEM micrographs analyzed in ImageJ. (D) Excitation wavelength-dependent fluorescence emission spectra of the CD; fluorescence emission data also revealed the quantum yield of the synthesized CD to be 47.8%. (E) Full survey XPS spectra and (F) high-definition C 1s spectra for the CD.

sputter coating with gold−palladium in a Denton Desk V Sputter Coater. Membrane surfaces were imaged in a Hitachi SU5000 Schottky Field-Emission SEM operating at an accelerating voltage of 5 kV. The cross-sectional morphology of the pristine and modified membranes was observed using SEM and TEM imaging. Additional information is in the Supporting Information. The attachment of the CD to the membrane surface was investigated for the pristine TFC, TFC-PDA, and CD-500 membranes by using X-ray photoelectron spectroscopy (XPS). Refer to the Supporting Information for more details.

The surface topography and roughness of pristine TFC and CD-100, CD-300, CD-500, and CD-1000 were evaluated by atomic force microscopy (AFM). Samples were cut into 10 mm × 10 mm squares and fixed with double-sided tape over a metal plate. Due to the samples' heterogeneity and rugosity, two approaches were used. Multimode 8 (Bruker) was used to scan small areas with a NanoscopeV electronic operating in peak force-tapping mode at a scan rate of 1.0 Hz, a probe with a spring constant of 0.4 N/m, and a resonance frequency of 70 kHz. The larger areas ($10 \times 10 \ \mu m^2$) were scanned using an NX-10 (ParkSystems) operating in tapping mode at a scan rate of 0.3 Hz, probe with a spring constant of 2.8 N/m, and resonance frequency of 75 kHz. Images were processed and analyzed using Gwyddion software (v. 2.53) to obtain average area roughness parameters such as root-mean-square height (S_q) and arithmetical mean height (S_a).

Surface hydrophilicity for pristine and modified TFC membranes was determined by using the sessile drop method with deionized water. Coupons of the TFC, TFC-PDA, and TFC-CD membranes were immobilized on glass microscope slides and dried overnight at room temperature. Following this, contact angle measurements were taken using a Theta Flex Optical Tensiometer (Biolin Scientific, Phoenix, AZ) and OneAttension software. The results are presented as the average of 50 measurements taken at random locations on the membrane coupons.

Intrinsic water transport properties such as water permeability (A) and solute permeability (B) were evaluated in a laboratory-scale cross-flow reverse osmosis system (Figure S1) following the procedures carefully described in our previous study.[10] The transport parameters A and B were determined for pristine TFC, TFC-PDA, CD-500, and CD-1000, the last two samples being the ones presenting the highest antimicrobial performance. The system was operated at 400 psi with a cross-flow velocity of 20 cm/s. Three different membrane coupons were tested for each sample. Other properties of the modified membrane, such as salt rejection and salt permeability, are calculated based on the collected intrinsic water transport performance data according to the following formula:

$$\text{desalination rate} = \frac{(\alpha - \beta)}{\alpha} \times 100\%$$

$$\text{salt penetration rate} = (1 - \text{salt rejection}) \times 100\%$$

where α is the salt content of reverse osmosis treatment influent water in mg/L and β is the salt content of reverse osmosis treatment effluent in mg/L.

Antibacterial Activity of Modified Membranes under Various Light Conditions. A plate counting method was employed to determine the antibacterial activity of CD-functionalized membranes, following previous studies[10,29] with some modifications. Experiments were performed using both Gram-negative *E. coli* (American Type Culture Collection ATCC 8739) and Gram-positive *B. subtilis* (American Type Culture Collection Strain 6633). Bacteria were grown overnight in Lysogenyl Broth (LB) in an incubator set to an appropriate temperature for the species utilized. The culture was then diluted in fresh LB (1:25) and grown under agitation and incubation at an appropriate temperature until the optical density at 600 nm (OD_{600}) reached 1.0, indicating a Log phase (∼2 h). Bacterial cells were washed three times by centrifugation at $5000g$ for 3 min using sterile saline (0.85% NaCl) before being diluted (1:10) to achieve a concentration of ∼10^8 colony-forming units (CFU) per mL.
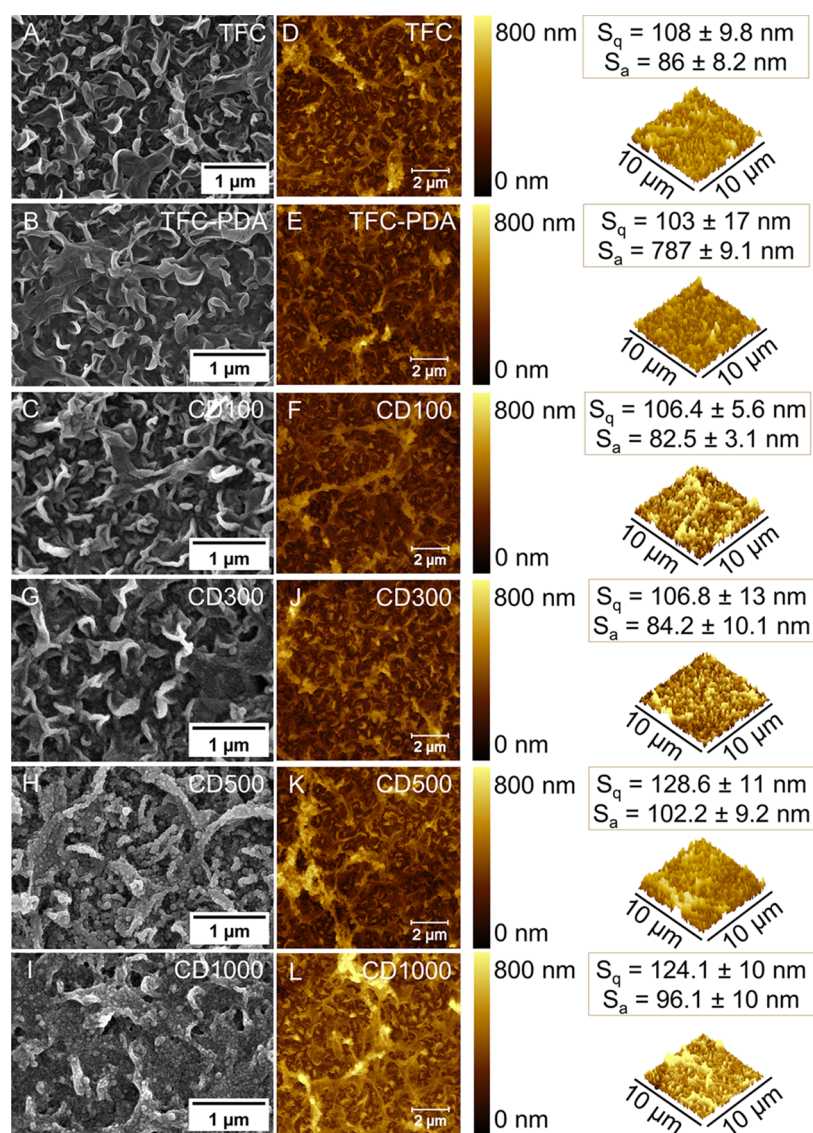
Figure 3. SEM micrographs of the (A) pristine TFC membrane (TFC), (B) membrane modified with only PDA (TFC-PDA), and (C, G−I) membrane modified with 100, 300, 500, and 1000 μg/mL of CD (CD-100, CD-300, CD-500, CD-1000). AFM topography images and 3D roughness mapping for the (D) pristine TFC membrane, (E) membrane modified with only PDA, and (F, J−L) CD-100, CD-300, CD-500, and CD-1000 membranes, respectively.

1.7 cm^2 coupons were cut from the TFC, TFC-PDA, CD-100, CD-300, CD-500, and CD-1000 membranes and then placed into poly(vinyl chloride) (PVC) holders so that only the polyamide active layer of the TFC membrane would be exposed to the bacterial suspension. Each membrane coupon was contacted with 5 mL of bacterial suspension (3 mL/cm^2) under one of three light conditions: darkness, simulated daylight (3500 K, 3.5 W LED lamp), or 365 nm UV light (3 W LED lamp). After 3 h, the bacterial suspension was discarded, and the membranes were carefully washed with 5 mL of sterile saline. The membrane coupons were bath-sonicated in 10 mL of sterile saline for 15 min to detach the bacteria from the membrane surface. 100 μL from each suspension was used for preparing serial dilutions, and 100 μL (10 × 10 μL droplets) of the bacteria suspension from each dilution was plated on an LB agar. Antimicrobial activity assays were conducted in quadruplicate, and the plates were incubated overnight before colonies were counted. In addition, the viability of *E. coli* cells attached to the CD-500 membrane surface following the 3 h contact time was quantified using fluorescent staining with SYTO 9 (live cells) and propidium iodide (PI, dead cells). Fluorescent-labeled membranes were observed using

confocal microscopy. Additional information is given in the Supporting Information.

Morphology of Bacteria Attached to the Membrane Surface. Suspensions of *E. coli* were prepared and exposed to the membrane surface following the method described above to evaluate the morphology of bacteria cells on the membrane surface. After contacting the membrane with the bacterial suspension, the membrane coupons were fixed and prepared for SEM imaging following the procedures described in our previous studies.[10,12]

Antibacterial Activity of TFC, TFC-PDA, and CD-500 Membranes after Prolonged Pre-Exposures to UV Light. To evaluate the antibacterial properties after repeated cycles of operation, modified membrane coupons were contacted with 5 mL of sterile saline under exposure to 365 nm UV light (3 W LED lamp) for 3, 6, 9, 15, and 24 consecutive hours. After the cycles of continuous light exposure were simulated, the modified TFC coupons were recovered, and their antibacterial properties were tested in darkness and under 365 nm UV light following the method described above.

Antibacterial Activity of the CD-Modified Membranes under Exposure to Synthetic Wastewater. Synthetic wastewater was formulated to replicate the characteristics of a secondary

wastewater effluent derived from conventional treatment plants. This synthetic composition comprised 8.0 mM NaCl, 0.2 mM CaCl$_2$, 0.15 mM MgSO$_4$, 0.4 mM NH$_4$Cl, 0.5 mM NaHCO$_3$, 0.2 mM KH$_2$PO$_4$, and 0.6 mM glucose, serving as the carbon source. The initial pH was maintained at 7.4 ± 0.5, while the conductivity stood at 1270 ± 76 μS·cm^{-1}. The antibacterial experiments were performed using *E. coli* following the method described above. One difference worth pointing out is that synthetic wastewater was used to prepare the 5 mL of bacterial suspension that would subsequently contact the membrane surface (3 mL/cm^2) during the 3 h exposure experiment.

RESULTS AND DISCUSSION

Physicochemical Characterization of Carbon Dots. The lignin-derived CD were prepared using an H$_2$O$_2$-assisted hydrothermal process. The visual presence of fluorescence under UV light (Figure 2A) was used to confirm the presence of the as-prepared CD in suspension qualitatively. In the TEM micrograph (Figure 2B), a well-distributed formation of uniform, nearly spherical CD can be observed. The average diameter of the nanoparticles, as measured from TEM micrographs using ImageJ software, was 10.7 ± 1.9 nm (Figure 2C).

To confirm that the fluorescence response observed was not caused by the lignin precursor material, fluorescence intensity at an excitation wavelength of 365 nm and an emission wavelength of 450 nm was recorded for both the CD suspension and bulk lignin suspended in DI water. The fluorescence intensity of the CD solution produced from the hydrothermal process was nearly 4 times that of the bulk lignin suspension at 360/450 nm (Figure S2B). Excitation wavelength-dependent fluorescence emission spectra (Figure 2D) were collected to determine the excitation wavelength that produced the strongest fluorescence response from the CD. The strongest fluorescence response was observed when the CD were excited at a wavelength of 380 nm. Following this excitation, mostly blue light was emitted, as indicated by the emission peak at ~470 nm. The quantum yield (QY) of CD (Figure 2D) was measured using the fluorescence emission spectra of CD and quinine sulfate dissolved in 0.050 M H$_2$SO$_4$ as a standard. QY indicates what percentage of the photons of the light absorbed by the CD are then emitted when the CD fluoresces. A QY of 47.8% was observed for the as-prepared CD. This result is considerably higher than the 9.2% reported for a similar one-pot, green synthesis method for CD.[55]

XPS analysis was performed on a lyophilized sample of the lignin-derived CD to characterize the CD surface functional groups and elemental composition (Figure 2E,F). On the full-survey graph for the lyophilized CD (Figure 2E), two prominent peaks can be observed at roughly 287 and 535 eV, corresponding to the C 1s and O 1s peaks, respectively. Hence, the major elemental components of the CD were carbon (61.9%) and oxygen (34.4%). Small amounts of sulfur (2.1%) and calcium (1.7%) were also observed in the elemental analysis, and their presence may be the result of impurities in the lignin used. The C 1s peak was deconvoluted into 4 peaks corresponding to C–C single bonds (284.8 eV), C–O single bonds (286.2 eV), C=O double bonds (288.1 eV), and O–C=O (289.9 eV) possibly from the presence of carboxylic acid functional groups on the surface of the CD.

Impact of Surface Functionalization on Membrane Properties. PDA chemistry was used to successfully attach the CD to the surface of the TFC membrane by PDA self-polymerization. Following the deposition of the initial PDA layer, a color change is observed in the solution contacting the

membrane surface. The solution goes from clear to brown in color, and this is indicative of the formation of PDA. For thicker layers of PDA formed after several hours of contact time, a brown color is also observed on the membrane surface, but not much color change was observed following the 15 min contact time for the initial PDA layer formation used herein. After functionalizing with CD, a color change from white to gray/brown was observed on all of the CD-modified membranes (Figure S3). CD deposition imparted a granular aspect to the membrane surface, and this morphology became more apparent as we increased the concentration of CD in solution during the membrane modification process (Figure 3A–C,G–I). A uniform distribution of CD nanoparticles can be observed on the surface of the CD-500 and CD-1000 modified membranes, as depicted in the SEM micrographs (Figure 3H,I). As noted, the color of the membrane surface became darker as the membrane was modified with increased CD concentrations, indicating improved CD deposition for the CD-500 and CD-1000 membranes.

The TFC membrane consists of two layers that include a polyamide film and a porous/support layer. The porous layer has a spongelike structure that can be easily seen in a cross-sectional SEM micrograph (Figure S4A), with a thickness of approximately 56 μm. The average thickness of the TFC polyamide selective layer was determined to be 84.7 ± 5.2 nm through cross-sectional TEM analysis using ImageJ software (Figure S4B). Upon application of CD to the membrane surface, the average thickness of the composite film increased to 235.8 ± 43.0 nm (Figure S4C), indicating the success of the modification protocol.

The surface topographies of the pristine and modified TFC membranes were evaluated by using AFM (Figure 3). The calculated root-mean-square height (S_q) and arithmetical mean height (S_a) for the pristine TFC membrane were 108 ± 9.8 and 86 ± 8.2 nm, respectively. The S_q and S_a for the TFC-PDA membrane were not significantly different than that of the control, at 103 ± 17 and 78.7 ± 9.1 nm, respectively. The thickness of the PDA layer formed is dependent upon the contact time between the surface and the buffered dopamine hydrochloride solution. In this study, the contact time was only 15 min, so only a thin layer of PDA formed, and that is likely the reason why the PDA layer did not significantly impact surface roughness. On the other hand, the uniform distribution of CD across the CD-500 and CD-1000 TFC membrane's polyamide active layer significantly increased the tridimensional surface roughness compared to pristine TFC and TFC-PDA membranes. CD-500 and CD-1000 membranes exhibited S_q and S_a values of 128.6 ± 11 and 102.2 ± 9.2 nm, and 124.1 ± 10 and 96.1 ± 10 nm, respectively (Figure 3K,L). S_q and S_a values for CD-100 and CD-300 did not show statistically significant differences from those of pristine TFC and TFC-PDA, which reflected the small number of CD nanoparticles present on the membrane surface. A similar increase in roughness was also reported by a previous study that modified the polysulfone support layer of TFC membranes with glucose-derived CD.[56]

The impact of CD deposition on membrane performance was determined by evaluating changes in the hydrophilicity of the TFC membranes. The modification of the TFC membranes with the initial thin layer of PDA was enough to reduce the water contact angle of the membranes from 36.5 ± 6.9° for the pristine membranes to 24.2 ± 5.7° for the TFC-PDA membrane (Figure 4A). Arena et al. also observed that
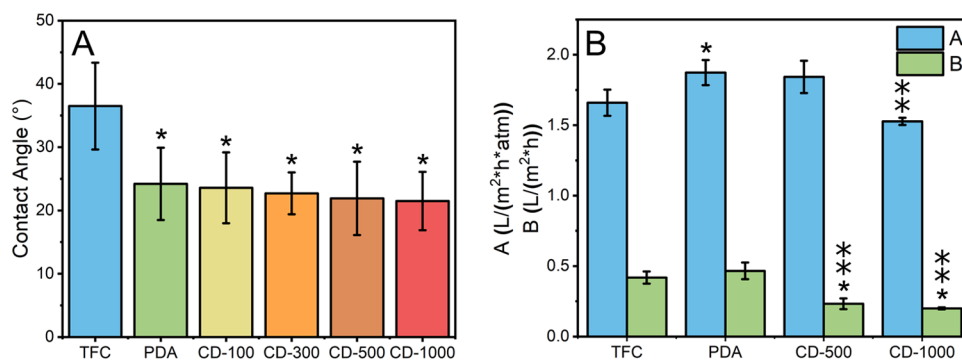
Figure 4. (A) Water contact angle of pristine TFC, TFC-PDA, and modified membranes (CD-100, CD-300, CD-500, and CD-1000). (B) Water permeability coefficient, *A*, and solute (NaCl) permeability coefficient, *B*, of TFC, TFC-PDA, CD-500, and CD-1000 membranes. An asterisk is used to denote samples that were statistically different from the control (pristine TFC) at a confidence level of 95% ($\alpha = 0.05$). Two vertically aligned asterisks denote samples that were statistically different from TFC-PDA.
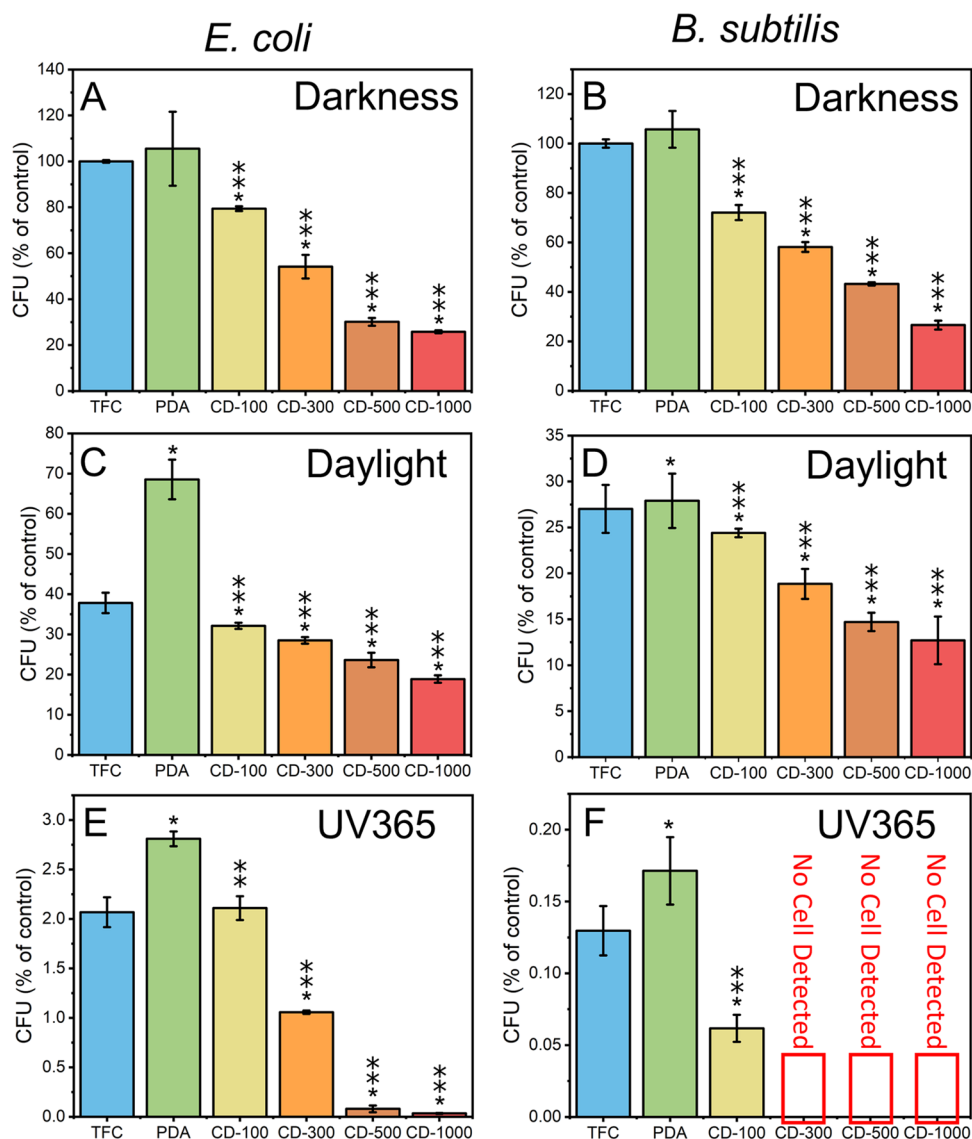
Figure 5. Antimicrobial properties of pristine and CD-functionalized membranes after exposure to *E. coli* cells (A, C, E) and *B. subtilis* cells (B, D, F) for 3 h in either darkness, simulated daylight, or 365 nm UV light. The CFU (% control) are expressed as viability percentages normalized to pristine TFC in darkness as the control. An asterisk denotes samples statistically different than their respective control tested at the same light condition at a confidence level of 95% ($\alpha = 0.05$). Two vertically aligned asterisks highlight samples statistically different from their respective TFC-PDA control.

functionalization with PDA alone can reduce the water contact angle of TFC membranes.[57] As CD were incorporated on the TFD-PDA membranes, we observed a slight decrease in contact angle for all of the CD-modified membranes. Although these contact angles for the CD-modified membranes were statistically different from those of the pristine TFC, they were found to be similar to that of TFC-PDA (95% confidence level, $\alpha = 0.05$). These results corroborate with the results presented by the XPS analysis that shows a higher content of oxygen for the TFC-PDA compared to pristine TFC or CD-500 membranes (Figure S6). The high-resolution XPS O 1s spectra show that the relative intensity of the peak centered at a binding energy of 530.5 eV (O−C=O) is greater for TFC-PDA (Figure S6G) than those of pristine TFC and CD-500 membranes (Figure S6C,E). This finding suggests that the functionalization with CD does not reduce the membrane hydrophilicity and the differences in contact angle are likely attributed to the presence of the PDA layer. A previous study by Ehtesabi et al. suggests that CD are highly hydrophilic and can be used to improve hydrophilicity,[58] but this may not extend to the modification method used herein or may depend on the properties of the CD synthesized.

The intrinsic transport properties of the pristine and functionalized membranes were evaluated in a bench-scale RO filtration system, and the results are shown in Figure 4B. Modification with PDA and CD slightly improved the water permeability of the TFC membranes. The pristine TFC membranes demonstrated a water permeability coefficient (A), of 1.66 ± 0.09 L/(m^2·h·atm). The water permeability coefficient of TFC-PDA was 1.87 ± 0.09 L/(m^2·h·atm), roughly 12.6% greater than that of the pristine TFC membrane, respectively. CD-500 or CD-1000 membranes did not show changes in the water permeability coefficient A compared to pristine TFC. However, when we compare the treatments with those of TFC-PDA, some differences emerge. For example, the water permeability coefficient A for CD-1000 membranes decreases significantly to 1.53 ± 0.03 L/(m^2·h·atm) when compared to TFC-PDA. Water flux changed from 45.2 ± 2.5 L·m^{-2}·h^{-1} for pristine TFC to 51.0 ± 2.4 and 50.2 ± 3.1 L·m^{-2}·h^{-1} for TFC-PDA and CD-500 membranes, respectively. However, this difference was not found to be statistically significant (Figure S5A). The water flux for the CD-1000 membrane (41.6 ± 0.7 L·m^{-2}·h^{-1}), although similar to that of pristine TFC, decreased significantly compared to that of TFC-PDA (51.0 ± 2.4 L·m^{-2}·h^{-1}).

Often, improvement in water permeability can be accompanied by a decrease in salt rejection.[59] But this was not the case with CD-500 and CD-1000 membranes. The B values for CD-500 and CD-1000 membranes were 0.23 ± 0.04 and 0.20 ± 0.04 L/(m^2·h), respectively, representing almost 50% reduction compared with pristine (0.42 ± 0.04 L/(m^2·h)) or TFC-PDA (0.47 ± 0.06 L/(m^2·h)) membranes. This difference means that CD-500 and CD-1000 show improved salt rejection compared to that of pristine and TFC-PDA membranes.

The decreased B values for CD-500 and CD-1000 membranes also translated into significant changes in NaCl penetration rates (%) (Figure S5B). For example, the NaCl penetration rate for CD-1000 (0.01%) decreased substantially compared with pristine TFC (0.02 ± 0.002%) and TFC-PDA (0.02 ± 0.003%). The desalination rates increased from 98.05 ± 0.17% for TFC to 98.93 ± 0.17 and 99.04 ± 0.03% for CD-500 and CD-1000 membranes, respectively. Despite the

increase in desalination rates for CD-500 and CD-1000 relative to the pristine TFC, no significant differences were observed for the same membranes when compared to TFC-PDA (Figure S5B).

Functionalized Membranes Exhibit Enhanced Antibacterial Activity. The antimicrobial properties of functionalized membranes were evaluated by exposing the membrane surface to *E. coli* and *B. subtilis* suspensions for 3 h in either darkness, simulated daylight, or 365 nm UV light. A plate counting method was used to determine the number and viability of attached cells, and the results of these antimicrobial assays are shown in Figure 5. The results in the dark environment showed that functionalization with CD imparted strong antibacterial activity to the membrane. As the CD concentration increased, the antibacterial ability of the CD-modified membranes also gradually increased for all of the tested conditions (e.g., darkness, daylight, and UV). In darkness, the percentage of bacterial inactivation for *E. coli* cells increased from 20.6 ± 1.04% for CD-100 to 74.2 ± 0.62% for CD-1000, showing more than a 3-fold increment in toxicity for CD-1000 compared to CD-100 (Figure 5A). A similar pattern was observed for the cells of *B. subtilis*. The CD-100 and CD-1000 could inactivate 27.9 ± 3.0 and 73.4 ± 1.8% of the cells under exposure to darkness, respectively, as depicted in Figure 5B. The TFC-PDA membrane displayed no toxicity to either *E. coli* or *B. subtilis* cells compared with the pristine TFC control. These results suggest that the amount of CD attached to the membrane surface directly impacts the antibacterial properties of the membranes of both *E. coli* and *B. subtilis*, regardless of the light condition applied.

Under simulated daylight, the pristine TFC membrane alone inactivated 62.2 ± 2.5 and 73.0 ± 2.6% of *E. coli* and *B. subtilis*, respectively, showing the light had a toxic effect itself (Figure 5C,D). CD-100 and CD-1000 membranes, when activated using the same simulated daylight, reduced the number of *E. coli* viable cells by 67.9 ± 4.9 and 81.1 ± 0.9%, respectively (Figure 5C). This result emphasized an increase in toxicity for membranes prepared using 1000 μg/mL rather than a 100 μg/mL CD suspension. Similarly, *B. subtilis* cells were inactivated by 75.6 ± 0.5 and 87.3 ± 2.6% by CD-100 and CD-1000 membranes under simulated daylight, demonstrating that CD-1000 was more toxic than its counterpart CD-100 (Figure 5D). Compared to darkness, the simulated day has been shown to be more effective in inactivating both *E. coli* and *B. subtilis* cells. This slight improvement may be due to the UV light component of the simulated daylight activating the CD on the membrane surface. While simulated sunlight is not the most effective for photoactivation of the as-prepared CD, it represents a more economical light source than energy-intensive UV lamps. Hence, the fact that simulated sunlight improves the antimicrobial activity of the CD-modified membranes represents a promising result when considering the application of these systems in real-life conditions.

The greatest bacterial deactivation was observed for membranes exposed to 365 nm UV light. After 3 h of exposure to 365 nm UV light, 97.9 ± 0.15% of *E. coli* and 99.87 ± 0.017% of *B. subtilis* were deactivated on the pristine TFC membrane surface. The CD-1000 membranes exposed to 365 nm UV light achieved near-complete sterilization (99.97 ± 0.045%) of *E. coli* cells within the 3 h contact time (almost 2 logs inactivation in addition to pristine TFC) (Figure 5E). The results of the antimicrobial activity assays for the TFC membranes against *B. subtilis* indicate that the CD-300, CD-
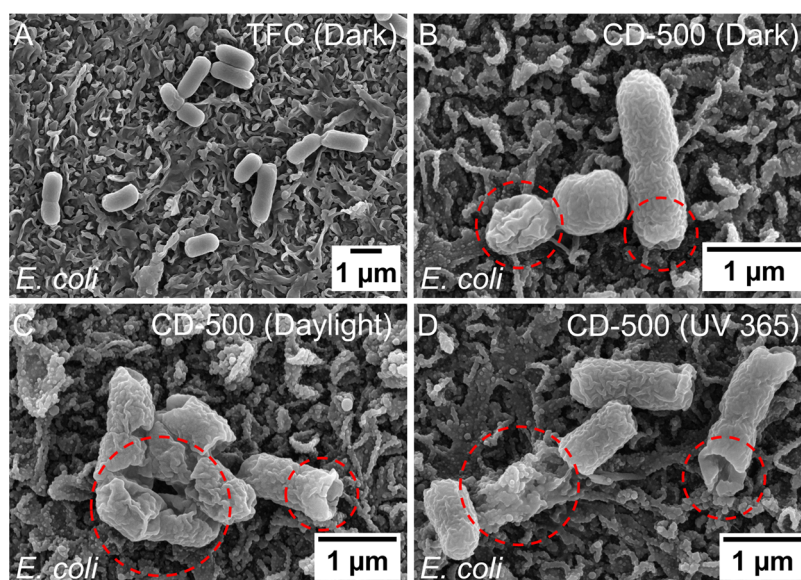
Figure 6. SEM micrographs showing the cellular integrity of *E. coli* cells after exposure to the TFC membrane in darkness (A), and the CD-500 membrane in darkness (B), daylight (C), and 365 nm UV light (D). Morphological damage to the *E. coli* cells is indicated with a red circle.

500, and CD-1000 membranes under UV light could nearly eliminate *B. subtilis* within the sensitivity limit of the plate counting technique employed (Figure 5F). Therefore, no *B. subtilis* colonies were observed after the sample was cultured from CD-300, CD-500, and CD-100 under 365 nm UV light for 3 h (Figure 5F). The findings depicted in Figure 5E,F confirm that the CD coating amplified the antimicrobial property under UV light exposure compared to the results obtained in darkness or simulated daylight. By comparing the four treatments (CD-100, CD-300, CD-500, and CD-1000) under the conditions tested, we found that the CD-1000 membranes had the highest level of toxicity. For example, although Figure 5E shows similar toxicity results for CD-500 and CD-1000, statistical analysis revealed that CD-1000 was significantly more toxic than CD-500 under 365 nm UV light. Considering the transport properties of the membranes, it was observed that both CD-500 and CD-1000 showed an increased salt rejection. However, CD-500 maintained the water permeability coefficient A intact, while CD-1000 presented significant losses in water permeability and water flux. Therefore, in contrast to CD-1000, the CD-500 membrane offers excellent antimicrobial activity without compromising the membrane transport properties.

The antibacterial properties of CD-500 were confirmed via a static biofouling assay in which *E. coli* cells attached to the membrane surface following the 3 h exposure time in darkness were then stained with the fluorescent markers SYTO 9 to label live cells and PI to label dead cells (Figure S7). A higher proportion of dead *E. coli* cells were attached to the CD-500 compared to the pristine TFC membrane. 32.0% of the *E. coli* cells attached to the pristine TFC membrane were dead, whereas 96.5% of the *E. coli* cells attached to the CD-500 membrane were labeled dead, as indicated by staining with PI (Table S1). SEM imaging was also used to confirm the presence of damaged cells (Figure 6) on the surface of the CD-500 membrane. For comparison, the undamaged *E. coli* cells on the pristine TFC membrane (no light exposure) can be seen in Figure 6A. We observe evident damage and loss of morphological integrity for the *E. coli* cells attached to CD-
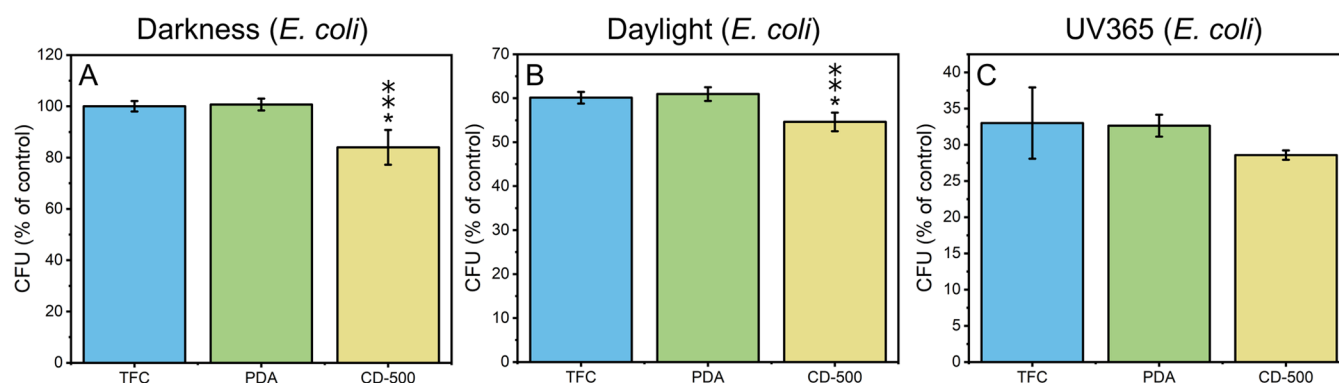
500 membranes exposed to darkness (Figure 6B). However, the loss of cell integrity is even more pronounced for the CD-500 membranes that were photoactivated with simulated daylight (Figure 6C) and 365 nm UV light (Figure 6D). Wrinkled, deformed cell membranes, holes in the cell membranes, and evidence of cell lysis can be observed (results highlighted by the red circles in the SEM images in Figure 6B–D).

The CD-modified membranes generally performed better against Gram-positive *B. subtilis* than Gram-negative *E. coli*, especially under UV light exposure. This disparity could be attributed to the differences between Gram-negative and Gram-positive bacteria. The cell membrane of Gram-negative is composed of a phospholipid bilayer inner cell membrane, a rigid peptidoglycan cell wall, and an outer phospholipid bilayer composed of lipopolysaccharides.[60] The extra outer cell membrane of Gram-negative bacteria may afford them more protection compared with the Gram-positive *B. subtilis*, which lacks this additional physical barrier. Gram-negative cells generally have a lower cell permeability than Gram-positive.[61] They also possess other mechanisms of protection, such as efflux pumps, that are absent in Gram-positive species. These differences in cell structure may be the reason for Gram-positive *B. subtilis* cells are more susceptible to chemical and physical means of inactivation by CD-functionalized membranes.

In contrast to the membrane surface functionalization with CD used herein, Zheng et al. were able to produce fouling-resistant thin-film nanocomposite (TFN) nanofiltration membranes by embedding CD modified with either cationic amine groups (PEI-CD) or anionic sulfonate groups (PS-CD) into the polyamide selective layer of the membranes.[62] These TFN membranes were able to overcome the previously discussed permeability-selectivity trade-off. By using ionic CD, they improved water permeability by creating charged nanovoids in the polyamide selective layer while enhancing the membrane's capacity to reject divalent ions due to Donnan and dielectric exclusion effects from the charge on the ionic CD. Improved membrane fouling resistance was observed for the
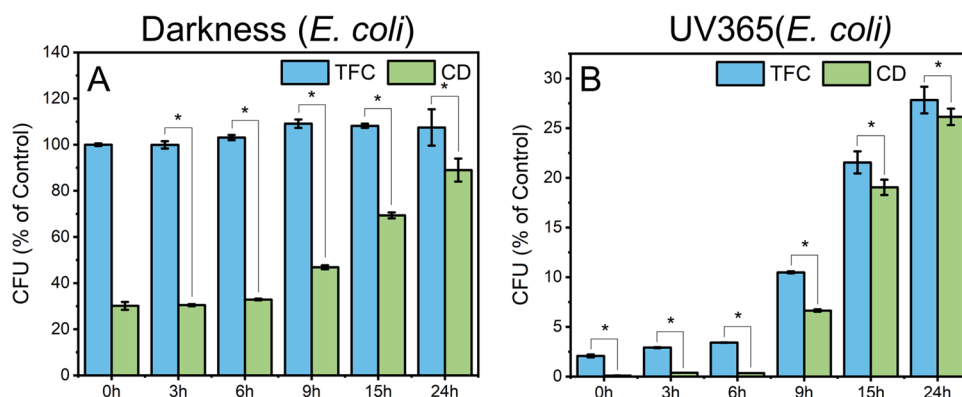
Figure 7. Antimicrobial properties of pristine TFC and CD-500 membranes after their pre-exposure to UV irradiation for prolonged periods (3, 6, 9, 15, and 24 h). After pre-exposure to UV light, the antibacterial activity of the membranes was tested in darkness (A) and under 365 nm UV light (B) using *E. coli* as a model microorganism. The CFU are expressed as viability percentages normalized to pristine TFC without 365 nm UV light exposure (TFC-0 h) in the dark as the control. One asterisk denotes that a sample significantly differs from its respective pristine TFC control at a confidence level of 95% (α = 0.05).

Figure 8. Antibacterial activity of pristine TFC, TFC-PDA, and CD-500 membranes exposed to synthetic wastewater under darkness (A), simulated daylight (B), and 365 nm UV light (C) using *E. coli* as a model organism. The CFU values are expressed as viability percentages normalized to pristine TFC treated in darkness. One asterisk and two vertically aligned asterisks denote a sample significantly different from the control pristine TFC and TFC-PDA, respectively, at a confidence level of 95% (α = 0.05).

membranes blended with the negatively charged PS-CD due to increased membrane hydrophilicity and stronger electrostatic repulsion between the membrane surface and the foulants. Another previous study used zwitterionic cyclodextrins to create a highly compact three-dimensional network of water channels in the polyamide layer of TFN membranes.[63] This resulted in fast water transport and effective salt ion repulsion. The study also found that the use of hydrophilic and zwitterionic groups improved the hydrophilicity and antifouling ability of the polyamide layer. The literature suggests that the antibacterial properties of our CD-modified membranes could be further enhanced by modifying the surface functional groups of CD to make them more anionic, which could repel negatively charged bacteria cells.[64]

In recent studies, the hypothetical mechanisms underlying the antimicrobial activity of CD against various microorganisms have been proposed.[40,65,66] A couple of key factors contribute to the mechanism of bacterial deactivation of CD. First, CD exhibit strong electrostatic interactions with bacterial cell membranes due to their surface functional groups (e.g., carboxyl groups), resulting in membrane deformation and disruption and loss in transport properties.[65] Second, under light irradiation, CD generate reactive oxygen species (ROS), which exacerbates oxidative stress within the bacterial cells.[40] This oxidative stress causes damage to vital cellular

components, such as proteins, lipids, and nucleic acids, ultimately leading to cell death.[66] Therefore, the cell toxicity observed for the TFC-CD membranes is likely the result of oxidative stress from the generation of ROS by the CD under photoactivation, but further work is needed to corroborate the underlying mechanism of action.

Antibacterial Properties of the CD-Modified Membranes Are Affected after Prolonged Exposure to UV Light. To assess the stability of the antimicrobial coating, we exposed the pristine TFC and CD-500 membrane to UV light over prolonged periods of time (3, 6, 9, 15, 18, and 24 h) before conducting the antimicrobial assays in darkness (Figure 7A) or under the presence of UV light for 3 h (Figure 7B). As the pre-exposure to UV light increased, we noticed a gradual decrease in the antimicrobial activity for the CD-500 sample tested under darkness (Figure 7A) and UV light (Figure 7B). For instance, after pre-exposing the CD-500 membrane to 365 nm UV light for 6 h, it retained over 95% of its antibacterial activity compared to its respective control tested under UV light (0 h UV365 sample) (Figure 7B). However, after being pre-exposed to 365 nm UV light for 9 h or longer, a substantial decline in the antibacterial effect is observed for CD-500 tested in darkness and under UV light (Figure 7A,B). To illustrate, CD-500 membranes pre-exposed to UV light for 9 h and tested under UV lost 24.0% in darkness and 6.6% under UV light of

their ability to inactivate *E. coli* cells compared to the control (0 h pre-exposure tested in UV light). In addition, when CD-500 membranes were pre-exposed to UV irradiation for 24 h, they demonstrated around 84.3% (darkness) and 26.1% (UV light) decreases in their antimicrobial activity compared to the CD-500 not pre-exposed but tested under UV light (0 h treatment tested in UV light). The data reveal that while the CD-500 membrane maintains a significant portion of its original toxicity under 6 h, its antibacterial efficacy will likely decline after continuous contact with UV light for 24 h or longer.

This decrease in toxicity under prolonged exposure to UV light can be attributed to a combination of factors. First, long-term exposure of CD to 365 nm UV light led to a gradual decrease in their fluorescence ability.[67] Second, extended irradiation caused changes in the surface characteristics of the CD-500 membrane (as seen in Figure S8), creating an environment conducive to the growth of bacterial colonies.[68,69] These changes affected the mechanism by which CD imparts toxicity, contributing to the observed decline in antibacterial performance. Therefore, in small-scale applications, careful calibration of the lighting source and its intensity is required. Additionally, adjusting the lighting distance is crucial to avoid any potential damage to the membrane. These operations are essential to maintain the structural integrity and functional performance of the membranes under practical application conditions.

CD-Modified Membranes Show Less Toxicity to Bacteria in the Presence of Simulated Wastewater. To evaluate the potential applicability of CD-modified membranes in real-world scenarios, we conducted antibacterial assays by replacing the saline solution (NaCl 0.9%) with synthetic wastewater (Figure 8). Synthetic wastewaters, unlike saline solutions, comprise a variety of electrolytes and carbon sources, making them a suitable medium for bacterial proliferation. Compared to the antibacterial results in saline solution, we observe that the antibacterial activity of the CD-500 membrane decreases upon contact with the simulated wastewater (Figure 8). This decrease in toxicity in the presence of simulated wastewater was observed across all tested conditions, including darkness (Figure 8A), simulated daylight (Figure 8B), and UV light (Figure 8C), but it was more pronounced for the CD-500 membranes tested under UV light. For example, in saline solution, CD-500 was found to inactivate almost 99.92 ± 0.03% of the cells within a 3 h time frame under UV light contact (Figure 6A). However, when exposed to synthetic wastewater, this toxicity drops to approximately 71.4 ± 0.6%, indicating a loss of approximately 28.5% in toxicity (Figure 8).

This decrease in toxicity can be attributed to two main factors. First, the bacteria present in the wastewater are more resilient to the toxic effects of CD-500 due to the availability of nutrients that support cellular growth. Second, the minerals and organic compounds present in the wastewater create a corona effect around the CD-500 particles on the membrane surface, ultimately affecting their capacity to absorb light and emit fluorescence, which in turn compromises their mechanisms of toxicity. These findings demonstrate the need to optimize the structure and catalytic properties of CD to maximize the utility of the CD-modified membranes in waters with fluctuating contents of organic matter and nutrients.

CONCLUSIONS

In this study, we produced lignin-derived and photoactive CD for applications as antibacterial agents. The CD nanoparticles were effective in imparting antibacterial properties to TFC membranes under different lighting conditions, including darkness, simulated daylight, and 365 nm UV light. We prepared four different CD-modified membranes using CD suspensions at different concentrations (100, 300, 500, and 1000 μg/mL), and we named them CD-100, CD-300, CD-500, and CD-1000. All four membranes showed antibacterial properties in darkness, indicating that the CD coating is active even in the absence of light. However, the toxicity of the CD-modified membranes improved significantly under exposure to simulated daylight and reached its maximum capacity under exposure to 365 nm UV light. Under UV light, the CD-modified membranes were highly toxic to both *E. coli* and *B. subtilis* cells but significantly more detrimental to *B. subtilis* cells. For example, CD-300, CD-500, and CD-1000 completely eliminated the attached *B. subtilis* under 365 nm UV light (no colonies detected in the plate counting). Among the four CD-based membranes tested, CD-500 and CD-1000 showed the highest antibacterial performances. However, CD-1000 revealed a decreased water permeability (parameter *A*) and water flux compared to those of CD-500 and the controls. We also studied the stability of the CD coating by pre-exposing CD-500 to continuous periods of UV irradiation (0, 3, 6, 9, 15, and 24 h). We found that the CD membrane showed no loss of antibacterial activity up to 6 h of continuous exposure to light. However, its toxicity declined drastically beyond 9 h of continuous treatment under 365 nm UV light, suggesting that the CD coating in CD-500, although functional in the first 6 h of operation, has its stability compromised under prolonged exposures to UV light. Finally, we tested the antimicrobial activity of CD-500 in simulated wastewater containing various electrolytes and glucose as a carbon source. The CD-500 membrane exposed to synthetic wastewater revealed a 28.5% loss in antibacterial effect compared to the same membrane tested in the presence of saline solutions. Our findings suggest that the CD membranes have potential applications under small-scale and controlled conditions. They also evidence the need to optimize the properties of CD further to improve their photocatalytic property and stability under UV irradiation.

ASSOCIATED CONTENT

Ⓢⓘ Supporting Information

The Supporting Information is available free of charge at https://pubs.acs.org/doi/10.1021/acsanm.3c05880.

> Materials and additional methods, a scheme for the RO filtration system, UV/visible light absorbance spectrum of CD, photos of pristine and modified membranes, results from cross-sectional morphology, salt penetration rate and desalination rate, XPS analyses of the pristine and CD-500 modified membranes, fluorescence images of bacteria on the TFC and CD-500 membrane surface, fluorescence microscopy images and cell counts from the static biofouling assay in darkness, and TFC membranes exposed to 365 nm UV light after repeated cycle experiments (PDF)

AUTHOR INFORMATION

Corresponding Author

Andreia F. Faria − *Engineering School of Sustainable Infrastructure & Environment, Department of Environmental Engineering Sciences, University of Florida, Gainesville, Florida 32611-6580, United States;* ● orcid.org/0000-0001-7473-040X; Phone: 352-392-7104; Email: andreia.faria@essie.ufl.edu

Authors

Liu Yang − *Engineering School of Sustainable Infrastructure & Environment, Department of Environmental Engineering Sciences, University of Florida, Gainesville, Florida 32611-6580, United States;* ● orcid.org/0009-0001-1666-9177

Jennifer C. Jackson − *Engineering School of Sustainable Infrastructure & Environment, Department of Environmental Engineering Sciences, University of Florida, Gainesville, Florida 32611-6580, United States*

Camilla H. M. Camargos − *Physical Chemistry Department, Institute of Chemistry, University of Campinas − UNICAMP, Campinas, São Paulo 13083-970, Brazil;* ● orcid.org/0000-0002-5240-036X

Marcella Torres Maia − *Solid-Biological Interface Group (SolBIN), Department of Physics, Federal University of Ceará − UFC, Fortaleza, Ceará 60455-900, Brazil; Brazilian Laboratory of Nanotechnology, National Center for Research in Energy and Materials − CNPEM, Campinas, São Paulo 13083-100, Brazil;* ● orcid.org/0000-0001-9489-4129

Diego Stéfani Teodoro Martinez − *Brazilian Laboratory of Nanotechnology, National Center for Research in Energy and Materials − CNPEM, Campinas, São Paulo 13083-100, Brazil*

Amauri Jardim de Paula − *Solid-Biological Interface Group (SolBIN), Department of Physics, Federal University of Ceará − UFC, Fortaleza, Ceará 60455-900, Brazil; Ilum School of Science, National Center for Research in Energy and Materials − CNPEM, Campinas, São Paulo 13083-100, Brazil;* ● orcid.org/0000-0002-3113-2597

Camila A. Rezende − *Physical Chemistry Department, Institute of Chemistry, University of Campinas − UNICAMP, Campinas, São Paulo 13083-970, Brazil;* ● orcid.org/0000-0002-2072-1361

Complete contact information is available at:
https://pubs.acs.org/10.1021/acsanm.3c05880

Notes

The authors declare no competing financial interest.

REFERENCES

(1) Elimelech, M.; Phillip, W. A. The Future of Seawater Desalination: Energy, Technology, and the Environment. *Science* **2011**, *333* (6043), 712−717.

(2) Lau, W. J.; Ismail, A. F.; Misdan, N.; Kassim, M. A. A Recent Progress in Thin Film Composite Membrane: A Review. *Desalination* **2012**, *287*, 190−199.

(3) Tang, C. Y.; Yang, Z.; Guo, H.; Wen, J. J.; Nghiem, L. D.; Cornelissen, E. Potable Water Reuse through Advanced Membrane Technology. *Environ. Sci. Technol.* **2018**, *52* (18), 10215−10223.

(4) Shannon, M. A.; Bohn, P. W.; Elimelech, M.; Georgiadis, J. G.; Marĩas, B. J.; Mayes, A. M. Science and Technology for Water Purification in the Coming Decades. *Nature* **2008**, *452* (7185), 301−310.

(5) Cohen-Tanugi, D.; McGovern, R. K.; Dave, S. H.; Lienhard, J. H.; Grossman, J. C. Quantifying the Potential of Ultra-Permeable Membranes for Water Desalination. *Energy Environ. Sci.* **2014**, *7* (3), 1134−1141.

(6) Uemura, T.; Himeshima, Y.; Kurihara, M. Interfacially Synthesized Reverse Osmosis Membrane. U.S. Patent US4761234A, 1979.

(7) Tang, C. Y.; Chong, T. H.; Fane, A. G. Colloidal Interactions and Fouling of NF and RO Membranes: A Review. *Adv. Colloid Interface Sci.* **2011**, *164*, 126 DOI: 10.1016/j.cis.2010.10.007.

(8) Rolf, J.; Cao, T.; Huang, X.; Boo, C.; Li, Q.; Elimelech, M. Inorganic Scaling in Membrane Desalination: Models, Mechanisms, and Characterization Methods. *Environ. Sci. Technol.* **2022**, *56*, 7484 DOI: 10.1021/acs.est.2c01858.

(9) Ang, W. S.; Tiraferri, A.; Chen, K. L.; Elimelech, M. Fouling and Cleaning of RO Membranes Fouled by Mixtures of Organic Foulants Simulating Wastewater Effluent. *J. Membr. Sci.* **2011**, *376* (1−2), 196 DOI: 10.1016/j.memsci.2011.04.020.

(10) Jackson, J. C.; Camargos, C. H. M.; Noronha, V. T.; Paula, A. J.; Rezende, C. A.; Faria, A. F. Sustainable Cellulose Nanocrystals for Improved Antimicrobial Properties of Thin Film Composite Membranes. *ACS Sustainable Chem. Eng.* **2021**, *9* (19), 6534−6540.

(11) Noronha, V. T.; Jackson, J. C.; Camargos, C. H. M.; Paula, A. J.; Rezende, C. A.; Faria, A. F. attacking-Attacking" Anti-Biofouling Strategy Enabled by Cellulose Nanocrystals-Silver Materials. *ACS Appl. Bio Mater.* **2022**, *5* (3), 1025 DOI: 10.1021/acsabm.1c00929.

(12) Noronha, V. T.; Camargos, C. H. M.; Jackson, J. C.; Souza Filho, A. G.; Paula, A. J.; Rezende, C. A.; Faria, A. F. Physical Membrane-Stress-Mediated Antimicrobial Properties of Cellulose Nanocrystals. *ACS Sustainable Chem. Eng.* **2021**, *9* (8), 3203 DOI: 10.1021/acssuschemeng.0c08317.

(13) Al-Juboori, R. A.; Yusaf, T. Biofouling in RO System: Mechanisms, Monitoring and Controlling. *Desalination* **2012**, *302*, 1 DOI: 10.1016/j.desal.2012.06.016.

(14) Hoek, E. M. V.; Weigand, T. M.; Edalat, A. Reverse Osmosis Membrane Biofouling: Causes, Consequences and Countermeasures. *npj Clean Water* **2022**, *5*, No. 45, DOI: 10.1038/s41545-022-00183-0.

(15) Flemming, H. C.; Schaule, G.; Griebe, T.; Schmitt, J.; Tamachkiarowa, A. Biofouling—the Achilles Heel of Membrane Processes. *Desalination* **1997**, *113* (2−3), 215−225.

(16) Flemming, H. C. Reverse Osmosis Membrane Biofouling. *Exp. Therm. Fluid Sci.* **1997**, *14* (4), 382−391.

(17) Saad, M. A. Biofouling Prevention in RO Polymeric Membrane Systems. *Desalination* **1992**, *88* (1−3), 85−105.

(18) Maddah, H.; Chogle, A. Biofouling in Reverse Osmosis: Phenomena, Monitoring, Controlling and Remediation. *Appl. Water Sci.* **2017**, *7* (6), 2637−2651.

(19) Xu, X.; Yang, Y.; Liu, T.; Chu, B. Cost-Effective Polymer-Based Membranes for Drinking Water Purification. *Giant* **2022**, *10*, No. 100099.

(20) Xu, R.; Wang, J.; Kanezashi, M.; Yoshioka, T.; Tsuru, T. Development of Robust Organosilica Membranes for Reverse Osmosis. *Langmuir* **2011**, *27* (23), 13996−13999.

(21) Chen, J.; Loeb, S.; Kim, J. H. LED Revolution: Fundamentals and Prospects for UV Disinfection Applications. *Environ. Sci.* **2017**, *3* (2), 188−202.

(22) Gora, S. L.; Rauch, K. D.; Ontiveros, C. C.; Stoddart, A. K.; Gagnon, G. A. Inactivation of Biofilm-Bound Pseudomonas Aeruginosa Bacteria Using UVC Light Emitting Diodes (UVC LEDs). *Water Res.* **2019**, *151*, 193−202.

(23) Ma, B.; Seyedi, S.; Wells, E.; McCarthy, D.; Crosbie, N.; Linden, K. G. Inactivation of Biofilm-Bound Bacterial Cells Using Irradiation across UVC Wavelengths. *Water Res.* **2022**, *217*, No. 118379.

(24) Guo, M.; Huang, J.; Hu, H.; Liu, W.; Yang, J. UV Inactivation and Characteristics after Photoreactivation of *Escherichia Coli* with Plasmid: Health Safety Concern about UV Disinfection. *Water Res.* **2012**, *46* (13), 4031−4036.

(25) Yin, J.; Yang, Y.; Hu, Z.; Deng, B. Attachment of Silver Nanoparticles (AgNPs) onto Thin-Film Composite (TFC) Membranes through Covalent Bonding to Reduce Membrane Biofouling. *J. Membr. Sci.* **2013**, *441*, 73−82.

(26) Kim, S. H.; Kwak, S. Y.; Sohn, B. H.; Park, T. H. Design of TiO2 Nanoparticle Self-Assembled Aromatic Polyamide Thin-Film-Composite (TFC) Membrane as an Approach to Solve Biofouling Problem. *J. Membr. Sci.* **2003**, *211* (1), 157−165.

(27) Xin, Q.; Shah, H.; Nawaz, A.; Xie, W.; Akram, M. Z.; Batool, A.; Tian, L.; Jan, S. U.; Boddula, R.; Guo, B.; Liu, Q.; Gong, J. R. Antibacterial Carbon-Based Nanomaterials. *Adv. Mater.* **2019**, *31* (45), No. 1804838.

(28) Mauter, M. S.; Elimelech, M. Environmental Applications of Carbon-Based Nanomaterials. *Environ. Sci. Technol.* **2008**, *42* (16), 5843−5859.

(29) Perreault, F.; Tousley, M. E.; Elimelech, M. Thin-Film Composite Polyamide Membranes Functionalized with Biocidal Graphene Oxide Nanosheets. *Environ. Sci. Technol. Lett.* **2014**, *1* (1), 71−76.

(30) Liu, Q.; Xu, G. R. Graphene Oxide (GO) as Functional Material in Tailoring Polyamide Thin Film Composite (PA-TFC) Reverse Osmosis (RO) Membranes. *Desalination* **2016**, *394*, 162−175.

(31) Ong, C. S.; Goh, P. S.; Lau, W. J.; Misdan, N.; Ismail, A. F. Nanomaterials for Biofouling and Scaling Mitigation of Thin Film Composite Membrane: A Review. *Desalination* **2016**, *393*, 2−15.

(32) Upadhyayula, V. K. K.; Gadhamshetty, V. Appreciating the Role of Carbon Nanotube Composites in Preventing Biofouling and Promoting Biofilms on Material Surfaces in Environmental Engineering: A Review. *Biotechnol. Adv.* **2010**, *28* (6), 802−816.

(33) Jastrzębska, A. M.; Kurtycz, P.; Olszyna, A. R. Recent Advances in Graphene Family Materials Toxicity Investigations. *J. Nanopart. Res.* **2012**, *14*, No. 1320. DOI: 10.1007/s11051-012-1320-8.

(34) Fadeel, B.; Bussy, C.; Merino, S.; Vázquez, E.; Flahaut, E.; Mouchet, F.; Evariste, L.; Gauthier, L.; Koivisto, A. J.; Vogel, U.; Martín, C.; Delogu, L. G.; Buerki-Thurnherr, T.; Wick, P.; Beloin-Saint-Pierre, D.; Hischier, R.; Pelin, M.; Candotto Carniel, F.; Tretiach, M.; Cesca, F.; Benfenati, F.; Scaini, D.; Ballerini, L.; Kostarelos, K.; Prato, M.; Bianco, A. Safety Assessment of Graphene-Based Materials: Focus on Human Health and the Environment. *ACS Nano* **2018**, *12* (11), 10582−10620.

(35) Eckelman, M. J.; Mauter, M. S.; Isaacs, J. A.; Elimelech, M. New Perspectives on Nanomaterial Aquatic Ecotoxicity: Production Impacts Exceed Direct Exposure Impacts for Carbon Nanotoubes. *Environ. Sci. Technol.* **2012**, *46* (5), 2902−2910.

(36) Lim, S. Y.; Shen, W.; Gao, Z. Carbon Quantum Dots and Their Applications. *Chem. Soc. Rev.* **2015**, *44* (1), 362−381.

(37) Kim, A.; Kim, J. H.; Patel, R. Modification Strategies of Membranes with Enhanced Anti-Biofouling Properties for Wastewater Treatment: A Review. *Bioresour. Technol.* **2022**, *345*, No. 126501.

(38) Li, H.; Huang, J.; Song, Y.; Zhang, M.; Wang, H.; Lu, F.; Huang, H.; Liu, Y.; Dai, X.; Gu, Z.; Yang, Z.; Zhou, R.; Kang, Z. Degradable Carbon Dots with Broad-Spectrum Antibacterial Activity. *ACS Appl. Mater. Interfaces* **2018**, *10* (32), 26936−26946.

(39) Fernando, K. A. S.; Sahu, S.; Liu, Y.; Lewis, W. K.; Guliants, E. A.; Jafariyan, A.; Wang, P.; Bunker, C. E.; Sun, Y. P. Carbon Quantum Dots and Applications in Photocatalytic Energy Conversion. *ACS Appl. Mater. Interfaces* **2015**, *7* (16), 8363−8376.

(40) Ghirardello, M.; Ramos-Soriano, J.; Galan, M. C. Carbon Dots as an Emergent Class of Antimicrobial Agents. *Nanomaterials* **2021**, *11* (8), 1877.

(41) Dong, X.; Liang, W.; Meziani, M. J.; Sun, Y. P.; Yang, L. Carbon Dots as Potent Antimicrobial Agents. *Theranostics* **2020**, *10* (2), 671.

(42) Varghese, M.; Balachandran, M. Antibacterial Efficiency of Carbon Dots against Gram-Positive and Gram-Negative Bacteria: A Review. *J. Environ. Chem. Eng.* **2021**, *9* (6), No. 106821.

(43) Meziani, M. J.; Dong, X.; Zhu, L.; Jones, L. P.; Lecroy, G. E.; Yang, F.; Wang, S.; Wang, P.; Zhao, Y.; Yang, L.; Tripp, R. A.; Sun, Y. P. Visible-Light-Activated Bactericidal Functions of Carbon "Quantum" Dots. *ACS Appl. Mater. Interfaces* **2016**, *8* (17), 10761−10766.

(44) Ragauskas, A. J.; Beckham, G. T.; Biddy, M. J.; Chandra, R.; Chen, F.; Davis, M. F.; Davison, B. H.; Dixon, R. A.; Gilna, P.; Keller, M.; Langan, P.; Naskar, A. K.; Saddler, J. N.; Tschaplinski, T. J.; Tuskan, G. A.; Wyman, C. E. Lignin Valorization: Improving Lignin Processing in the Biorefinery. *Science* **2014**, *344*, No. 1246843, DOI: 10.1126/science.1246843.

(45) Kang, C.; Huang, Y.; Yang, H.; Yan, X. F.; Chen, Z. P. A Review of Carbon Dots Produced from Biomass Wastes. *Nanomaterials* **2020**, *10*, 2316 DOI: 10.3390/nano10112316.

(46) Wang, D.; Lee, S. H.; Kim, J.; Park, C. B. Waste to Wealth": Lignin as a Renewable Building Block for Energy Harvesting/Storage and Environmental Remediation. *ChemSusChem* **2020**, *13*, 2807 DOI: 10.1002/cssc.202000394.

(47) Camargos, C. H. M.; Rezende, C. A. Antisolvent versus Ultrasonication: Bottom-up and Top-down Approaches to Produce Lignin Nanoparticles (LNPs) with Tailored Properties. *Int. J. Biol. Macromol.* **2021**, *193*, 647−660.

(48) Sims, R.; Taylor, M.; Saddler, J.; Mabee, W. *From 1st- to 2nd-Generation Biofuel Technologies* IEA; 2008.

(49) Zhuang, J.; Ren, S.; Zhu, B.; Han, C.; Li, Y. Y.; Zhang, X.; Gao, H.; Fan, M.; Tian, Q. Lignin-Based Carbon Dots as High-Performance Support of Pt Single Atoms for Photocatalytic H2 Evolution. *Chem. Eng. J.* **2022**, *446*, No. 136873.

(50) Si, M.; Zhang, J.; He, Y.; Yang, Z.; Yan, X.; Liu, M.; Zhuo, S.; Wang, S.; Min, X.; Gao, C.; Chai, L.; Shi, Y. Synchronous and Rapid Preparation of Lignin Nanoparticles and Carbon Quantum Dots from Natural Lignocellulose. *Green Chem.* **2018**, *20* (15), 3414−3419.

(51) Chen, W.; Hu, C.; Yang, Y.; Cui, J.; Liu, Y. Rapid Synthesis of Carbon Dots by Hydrothermal Treatment of Lignin. *Materials* **2016**, *9* (3), 184 DOI: 10.3390/ma9030184.

(52) Camargos, C. H. M.; Rezende, C. A. Structure−Property Relationships of Cellulose Nanocrystals and Nanofibrils: Implications for the Design and Performance of Nanocomposites and All-Nanocellulose Systems. *ACS Appl. Nano Mater.* **2021**, *4* (10), 10505−10518.

(53) Lee, H.; Dellatore, S. M.; Miller, W. M.; Messersmith, P. B. Mussel-Inspired Surface Chemistry for Multifunctional Coatings. *Science* **2007**, *318* (5849), 426−430.

(54) Ball, V.; Frari, D. D.; Toniazzo, V.; Ruch, D. Kinetics of Polydopamine Film Deposition as a Function of PH and Dopamine Concentration: Insights in the Polydopamine Deposition Mechanism. *J. Colloid Interface Sci.* **2012**, *386* (1), 366−372.

(55) Yuan, M.; Zhong, R.; Gao, H.; Li, W.; Yun, X.; Liu, J.; Zhao, X.; Zhao, G.; Zhang, F. One-Step, Green, and Economic Synthesis of Water-Soluble Photoluminescent Carbon Dots by Hydrothermal Treatment of Wheat Straw, and Their Bio-Applications in Labeling, Imaging, and Sensing. *Appl. Surf. Sci.* **2015**, *355*, 1136 DOI: 10.1016/j.apsusc.2015.07.095.

(56) Li, Y.; Li, S.; Zhang, K. Influence of Hydrophilic Carbon Dots on Polyamide Thin Film Nanocomposite Reverse Osmosis Membranes. *J. Membr. Sci.* **2017**, *537*, 42−53.

(57) Arena, J. T.; McCloskey, B.; Freeman, B. D.; McCutcheon, J. R. Surface Modification of Thin Film Composite Membrane Support Layers with Polydopamine: Enabling Use of Reverse Osmosis Membranes in Pressure Retarded Osmosis. *J. Membr. Sci.* **2011**, *375* (1−2), 55−62.

(58) Ehtesabi, H.; Massah, F. Improvement of Hydrophilicity and Cell Attachment of Polycaprolactone Scaffolds Using Green Synthesized Carbon Dots. *Mater. Today Sustainability* **2021**, *13*, No. 100075.

(59) Park, H. B.; Kamcev, J.; Robeson, L. M.; Elimelech, M.; Freeman, B. D. Maximizing the Right Stuff: The Trade-off between Membrane Permeability and Selectivity. *Science* **2017**, *356* (6343), 1138−1148.

(60) Silhavy, T. J.; Kahne, D.; Walker, S. The Bacterial Cell Envelope. *Cold Spring Harbor Perspect. Biol.* **2010**, *2*, No. a000414, DOI: 10.1101/cshperspect.a000414.

(61) Reygaert, W. C. An Overview of the Antimicrobial Resistance Mechanisms of Bacteria. *AIMS Microbiol.* **2018**, *4* (3), 482.

(62) Zheng, H.; Mou, Z.; Lim, Y. J.; Liu, B.; Wang, R.; Zhang, W.; Zhou, K. Incorporating Ionic Carbon Dots in Polyamide Nanofiltration Membranes for High Perm-Selectivity and Antifouling Performance. *J. Membr. Sci.* **2023**, *672*, 121401 DOI: 10.1016/j.memsci.2023.121401.

(63) Zheng, H.; Mou, Z.; Zhou, K. Incorporation of Core-Shell-Structured Zwitterionic Carbon Dots in Thin-Film Nanocomposite Membranes for Simultaneously Improved Perm-Selectivity and Antifouling Properties. *ACS Appl. Mater. Interfaces* **2020**, *12* (47), 53215 DOI: 10.1021/acsami.0c13386.

(64) Li, Z.; Ma, J.; Ruan, J.; Zhuang, X. Using Positively Charged Magnetic Nanoparticles to Capture Bacteria at Ultralow Concentration. *Nanoscale Res. Lett.* **2019**, *14*, No. 195, DOI: 10.1186/s11671-019-3005-z.

(65) Guo, B.; Liu, G.; Hu, C.; Lei, B.; Liu, Y. The Structural Characteristics and Mechanisms of Antimicrobial Carbon Dots: A Mini Review. *Mater. Adv.* **2022**, *3* (21), 7726−7741.

(66) Yu, M.; Li, P.; Huang, R.; Xu, C.; Zhang, S.; Wang, Y.; Gong, X.; Xing, X. Antibacterial and Antibiofilm Mechanisms of Carbon Dots: A Review. *J. Mater. Chem. B* **2023**, *11* (4), 734−754.

(67) Dua, S.; Kumar, P.; Pani, B.; Kaur, A.; Khanna, M.; Bhatt, G. Stability of Carbon Quantum Dots: A Critical Review. *RSC Adv.* **2023**, *13*, 13845 DOI: 10.1039/D2RA07180K.

(68) Rho, H.; Im, S. J.; Alrehaili, O.; Lee, S.; Jang, A.; Perreault, F.; Westerhoff, P. Facile Surface Modification of Polyamide Membranes Using UV-Photooxidation Improves Permeability and Reduces Natural Organic Matter Fouling. *Environ. Sci. Technol.* **2021**, *55* (10), 6984 DOI: 10.1021/acs.est.0c07844.

(69) Rho, H.; Yu, P.; Zhao, Z.; Lee, C. S.; Chon, K.; Perreault, F.; Alvarez, P. J. J.; Amy, G.; Westerhoff, P. Inhibition of Biofouling on Reverse Osmosis Membrane Surfaces by Germicidal Ultraviolet Light Side-Emitting Optical Fibers. *Water Res.* **2022**, *224*, 119094 DOI: 10.1016/j.watres.2022.119094.